Int. J. Heat Mass Transfer. Vol. 29, No. 8, pp. 1149–1158, 1986
Printed in Great Britain

0017–9310/86 $3.00 + 0.00
Pergamon Journals Ltd.

Droplet deposition in two-phase, turbulent flow

M. M. EL-KASSABY* and E. N. GANIĆ†

* Faculty of Engineering, Alexandria University, Alexandria, Egypt
† Faculty of Mechanical Engineering, University of Sarajevo, Post Fah 107, Sarajevo 71000, Yugoslavia

Abstract—Theoretical and experimental studies have been carried out to investigate further the turbulent deposition of particles from two-phase droplet flow onto the smooth wall of a vertical tube. The work of Ganić and Mastanaiah [*Int. J. Multiphase Flow* 7, 401–422 (1981)] for the Stokes regime has been extended by this study to include the Oseen regime ($Re_p \leqslant 5$). The proposed theory satisfactorily describes the existing data, as well as the new data taken for air–water droplet flow passing through a 12.95-mm-diameter stainless-steel tube at $Re = 27\,000$, 36 000, 43 000 and 55 000.

1. INTRODUCTION

THE DETERMINATION of droplet deposition rates is of interest in many applications, such as steam generators and nuclear reactor cooling systems. In two-phase turbulent gas and particle flow through a vertical tube having a diameter in excess of about a micron, deposition on the wall occurs primarily by turbulent diffusion, in the absence of electrostatic effects and large temperature gradients.

The experimental deposition data are usually presented in terms of a dimensionless deposition velocity k_d/U^* as a function of the dimensionless particle relaxation time τ^+, based on the Stokes drag force, defined as

$$\tau^+ = \frac{d_p^2 \rho_g \rho_p U^{*2}}{18\mu_g^2}. \tag{1}$$

In many practical two-phase flow problems, the deposition of large particles having d_p in excess of about 20–30 μm is of interest. (A review of various theoretical and experimental studies on the deposition of large particles was made recently by Ganić and Mastanaiah [1].) For vertical flow systems, deposition data in this range include those developed by Sehmel [2], Ilori [3], Forney and Spielman [4], Liu and Agarwal [5] and Agarwal [6] for uniform-sized particles, and Cousins and Hewitt [7] and Farmer *et al.* [8] involving drop size distribution.

For theoretical analyses of the deposition of particles in the above range, see Friedlander and Johnstone [9], Forney and Spielman [4], Cleaver and Yates [10], Namie and Ueda [11] and Hagiward and Satao [12]. The various limitations of the above models and the conceptual deficiencies associated with them are described in detail by Ganić and Mastanaiah [1], who have proposed a physically more acceptable model for the deposition motion. The latter model considers that for large particles with a dimensionless stopping distance (based on Stokes drag) $S^+ > 30$, the particles move from the tube center to the periphery of the buffer layer by turbulent diffusion, then reach the wall by free flight, owing to the inertia imparted to them by the turbulent eddies at the start of their free flight. Their analysis, using Tchen's theory [13] for particle diffusion was valid within the Stokes regime. The main limitation of their theory is that it cannot be applied to particles outside the Stokes regime, i.e. $Re_p > 1$, where

$$Re_p = \rho_g \frac{|V_p - V_g| d_p}{\mu_g} \tag{2}$$

where V_p and V_g represent r.m.s. velocity fluctuation of particle and fluid, respectively. The main purpose of the present work is to extend the above theory to include the Oseen regime ($Re_p \leqslant 5$).

2. THEORETICAL ANALYSIS

The physical model used here for the deposition of large particles is similar to that proposed by Ganić and Mastanaiah [1]. The most important difference between the present work and the above is in the calculation of the particle to fluid diffusivity ratio, δ.

2.1. *Deposition velocity*

The following assumptions, originally made by Mastanaiah [14], are repeated with some revisions in the analysis here.

(a) The flow is fully developed.
(b) The concentration profile is developed so that the entrance effects are not present.
(c) Drop concentration is so small that it may be considered that the fluid turbulence characteristics are unaltered.
(d) Particle size is such that the explanation of its motion relative to the fluid includes the Oseen regime ($Re_p \leqslant 5$).

NOMENCLATURE

C drop (particle) concentration [kg m^{-3}]
$\bar{C}$ bulk concentration $w_d/(w_g/\rho_g + w_d/\rho_d)$ [kg m^{-3}]
C_D drag coefficient
C_c centerline concentration [kg m^{-3}]
D tube diameter [m]
d_p droplet diameter [m]
E entrainment
F fractional deposition
f smooth tube friction factor, $2\tau_w/(\rho_g \bar{U}^2)$
g acceleration due to gravity [m s^{-2}]
k_d deposition velocity [m s^{-1}]
k_d^+ dimensionless deposition velocity, k_d/U^*
L tube length [m]
m droplet mass [kg]
N local rate of radial mass flux of droplets [kg m^{-2} s^{-1}]
N_o mass rate of deposition of droplets [kg m^{-2} s^{-1}]
r radial distance from the tube center [m]
r_o tube inner radius [m]
r_o^+ $U^* r_o/\nu_g$
S stopping distance based on Stokes drag, $d_p^2 \rho_p V_{po}/18\mu_g$
S^+ dimensionless stopping distance, SU^*/ν_g
t time [s]
$\bar{U}$ superficial mean gas velocity [m s^{-1}]
U^+ U/U^*
U^* friction velocity, $\bar{U}\sqrt{f/2}$ [m s^{-1}]
V_g radial r.m.s. fluctuating velocity of gas [m s^{-1}]
V_g' radial fluctuating velocity of gas [m s^{-1}]
V_p radial r.m.s. fluctuating velocity of drop [m s^{-1}]
V_p' radial fluctuating velocity of drop [m s^{-1}]
V_{po} value of V_p at start of free flight ($y^+ = 30$) [m s^{-1}]
y radial distance from wall surface [m]
y^+ dimensionless radial distance, $U^* y/\nu_g$
w $V_g - V_p$ [m s^{-1}].

Greek symbols

δ particle to fluid diffusivity ratio, $\varepsilon_p/\varepsilon_f$
ε_g fluid diffusivity [m^2 s^{-1}]
ε_p particle diffusivity [m^2 s^{-1}]
μ dynamic viscosity [N s m^{-2}]
ν kinematic viscosity [m^2 s^{-1}]
τ drop relaxation time based on Stokes drag, S/V_{po}
τ^+ dimensionless drop relaxation time, $\tau U^{*2}/\nu_g$
τ_w wall-shear stress [N m^{-2}].

Subscripts

c centerline
d droplet
g gas phase, bulk, air–water vapor mixture
p drop (particle).

(e) There is no wall rebound or re-entrainment of drops.
(f) The local mass flux of droplets in the turbulent core varies linearly from zero at the tube center to a value of N_o at $y^+ = 30$, thus remaining constant to a value equal to N_o in the region $0 < y^+ < 30$. Therefore, the local mass flux can be given as

$$N = \frac{N_o}{1-(30/r_o^+)}\left(1 - \frac{y^+}{r_o^+}\right). \tag{3}$$

(g) Both the fluid and the droplet move radially towards the wall with the radial r.m.s. fluctuating velocity.

The rate law for the diffusion of droplets is given by

$$N = \varepsilon_p \frac{dC}{dy} \tag{4}$$

where ε_p is the particle diffusivity and equal to $\delta\varepsilon_g$. Equation (4) for the particle flux is based on the assumption that the particles in the gas core interact with the turbulent eddies in such a way that particle dispersion is considered essentially diffusive. The eddy diffusivity (ε_g) expression proposed by Reichardt [15] is also considered here and is given by

$$\varepsilon_g = \frac{K r_o U^*}{6}\left[1 - \left(\frac{r}{r_o}\right)^2\right]\left[1 + 2\left(\frac{r}{r_o}\right)^2\right]. \tag{5}$$

Here K is the mixing length constant and is equal to 0.4. Integration of equation (4) between $y^+ = 30$ and a point y^+ in the core leads to the concentration distribution as given by

$$C - C_b = \frac{N_o}{[1-(30/r_o^+)]\,U^*\delta K} \times \ln\left[\frac{1+2x}{1-x}\right]_{x=(1-30/r_o^+)}^{x=(1-y^+/r_o^+)}. \tag{6a}$$

At $y^+ = r_o^+$, we have

$$C_c - C_b = \frac{N_o}{[1-(30/r_o^+)]\,U^*\delta K} \times \ln\left\{\frac{1+2[1-(30/r_o^+)]^2}{1-[1-(30/r_o^+)]^2}\right\}. \tag{6b}$$

The deposition velocity is defined as

$$k_d = \frac{N_o}{\bar{C}} \tag{7a}$$

with the bulk concentration $\bar{C}$ given by

$$\bar{C} = \frac{\int_0^{r_o} CUr\,dr}{\int_0^{r_o} Ur\,dr} \tag{7b}$$

where $U(r)$ is the radial velocity distribution in the tube [16]. In evaluating $\bar{C}$, it is assumed that $C = C_b$ for $0 < y^+ < 30$. This assumption was studied in detail by Ganić and Mastanaiah [1]. Following the same procedure (see [1, equations (5)–(7)] to find $C_c/\bar{C}$), the expression for the deposition velocity is obtained in the dimensionless form as:

$$\frac{k_d}{U^*} = \delta(C_c/\bar{C}) \Big/ \left\{ \frac{2.5}{1-(30/r_o^+)} \times \ln\left[\frac{1+(1+2[1-(30/r_o^+)])^2}{1-[1-(30/r_o^+)]^2}\right] + \sqrt{\frac{\delta}{0.75}} \right\} \tag{8}$$

2.2. *Particle to fluid diffusivity ratio* δ

The diffusivity ratio δ is defined as [17]

$$\delta = \varepsilon_p/\varepsilon_q = \overline{V_p'^2}/\overline{V_g'^2} = V_p^2/V_g^2. \tag{9}$$

The diffusivity ratio, δ, can be determined from the equation of motion of the particles in a turbulent flow field, neglecting the gravitational and pressure gradient forces. Taking into consideration the assumption number g, the equation of motion can be written as

$$m\frac{dV_p}{dt} = C_D\frac{\pi d_p^2}{8}\rho_g(V_g - V_p)^2 \tag{10a}$$

where the drag coefficient C_D was taken for the Oseen regime [18], which is valid up to $Re_p = 5$, as

$$C_D = \frac{24}{Re_p}\left(1 + \frac{3}{16}Re_p\right). \tag{10b}$$

Substituting equation (2) into (10b) and then into (10a), we get

$$\frac{dV_p}{dt} = a|V_g - V_p| + b(V_g - V_p)^2 \tag{11a}$$

where

$$a = \frac{18\mu_g}{d_p^2\rho_p} \tag{11b}$$

and

$$b = \frac{27\rho_g}{8d_p\rho_p}. \tag{11c}$$

If $V_g - V_p = w$, then equation (11a) can be rewritten as

$$\frac{dw}{dt} = -bw^2 - aw + \frac{dV_g}{dt}. \tag{12}$$

To solve the last differential equation, we have to know dV_g/dt. For the time being, let $dV_g/dt = C_1$ (see Section 2.4) and then we can use the Riccati technique [19] to convert equation (12) from nonlinear form, as follows.

Let

$$w = \frac{\xi'}{b\xi} \tag{13}$$

then

$$\frac{dw}{dt} = \frac{b\xi\xi'' - b\xi'^2}{(b\xi)^2}. \tag{14}$$

Substituting into equation (12), we obtain

$$\xi'' + a\xi' - b\xi C_1 = 0 \tag{15}$$

which is an ordinary differential equation, having the general solution

$$\xi = K_2 e^{C_3 t} + K_3 e^{C_4 t} \tag{16}$$

provided that $dV_g/dt > 0$ (see Fig. 1) where

$$C_3 = -\frac{a}{2} + \frac{1}{2}\sqrt{a^2 + 4bC_1} \tag{17a}$$

$$C_4 = -\frac{a}{2} - \frac{1}{2}\sqrt{a^2 + 4bC_1}. \tag{17b}$$

The constants K_2 and K_3 can be determined from the boundary condition.

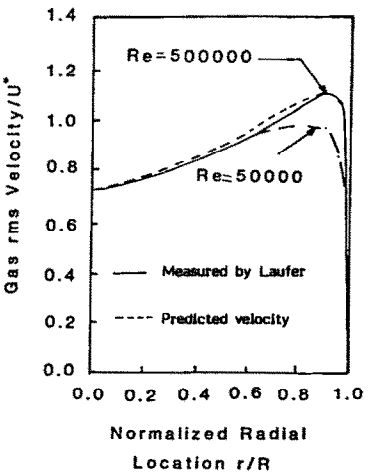

FIG. 1. Comparison between the measured value of the r.m.s. velocity and the predicted value.

Equation (13) can be rewritten as

$$w = \frac{1}{b}\left(\frac{K_2 C_3 e^{C_3 t} + K_3 C_4 e^{C_4 t}}{K_2 e^{C_3 t} + K_3 e^{C_4 t}}\right) \tag{18}$$

assuming that the boundary condition at the centerline is as follows:

$$\text{at} \quad t = 0, \quad w = w_o \tag{19a}$$

where $w_o = w$ at the centerline. This boundary condition gives

$$K_2 = K_3 C_5 \tag{19b}$$

where

$$C_5 = \frac{C_4 - w_o b}{w_o b - C_3}. \tag{19c}$$

Substituting equations (19c) and (19b) into (18), we get

$$V_g - V_p = w = \frac{1}{b}\left(\frac{C_5 C_3 e^{C_3 t} + C_4 e^{C_4 t}}{C_5 e^{C_3 t} + e^{C_4 t}}\right). \tag{20}$$

The selection of the initial condition w_o is discussed in detail by El-Kassaby [20], and in the range of the present data ($6000 < Re < 50\,000$), w_o is selected to be $0.2U^*$.

2.3. *The stopping distance and the relaxation time*

The stopping distance S is defined as the distance a particle would travel through a stagnant fluid ($V_g = 0$) with a prescribed velocity. Considering equation (12a), the stopping distance can be derived as

$$S = \frac{1}{b}\ln\left(\frac{a + bV_{po}}{a}\right) \tag{21a}$$

where V_{po} is the free flight velocity at the edge of the buffer layer taken as $0.9U^*$ [9]. Equation (21a) can be written in dimensionless form as follows:

$$S^+ = \frac{SU^*}{\nu_g} = \frac{18 d_p \rho_p U^*}{27 \mu_g}\ln\left(1 + \frac{2.7 \rho_g d_p U^*}{16 \mu_g}\right). \tag{21b}$$

The relaxation time τ can be expressed as follows

$$\tau = \frac{S}{V_{po}} \tag{22a}$$

which can be rewritten in nondimensional form as follows

$$\tau^+ = \frac{\tau U^{*2}}{\nu_g} = 0.3292 \frac{d_p U^*}{\nu_g}\ln\left(1 + \frac{2.7 d_p U^*}{16 \nu_g}\right). \tag{22b}$$

2.4. *Verification of the assumption* $dV_g/dt = C_1$

Measurements by Laufer [21] have shown that the distribution of V_g vs the radial distance is almost the same for different Re, in the range $1 \geqslant y/r_o \geqslant 0.1$ (Fig. 1), and for this range V_g is varying from $0.72U^*$ at the centerline up to $1.1U^*$ at $y/r_o \simeq 0.1$, which will be used later as a boundary condition. From the previous analysis and referring to Fig. 1, it can be shown that over almost the whole radial distance, the relation of V_g/U^* vs r/r_o can be represented by a parabolic relation which predicts a linear relationship with respect to time. The above-mentioned fact was the main idea used in solving equation (12) by setting

$$\frac{dV_g}{dt} = C_1. \tag{23}$$

Equation (23) can be rewritten as follows:

$$V_g \frac{dV_g}{dr} = C_1. \tag{24}$$

By integrating (24) we get

$$\frac{V_g^2}{2} = C_1 r + C_6 \tag{25}$$

where C_6 is constant, depending on the boundary condition.

Knowing that $r = r_o - y$, then

$$\frac{V_g^2}{2} = C_1 r_o\left(1 - \frac{y}{r_o}\right) + C_6. \tag{26}$$

Multiplying the previous equations by U^*/ν_g, to get them in dimensionless form, we obtain

$$\frac{V_g^2}{2}\frac{U^*}{\nu_g} = C_1 r_o^+\left(1 - \frac{y^+}{r_o^+}\right) + C_6 \frac{U^*}{\nu_g}. \tag{27}$$

Using the boundary condition as measured by Laufer [21] (see Fig. 1), it follows that:

$$\left.\begin{aligned} &V_g = 0.72U^*, \quad \text{at the centerline} \\ \text{and} \\ &V_g = 1.1U^*, \quad \text{at } y/r_o \simeq 0.1. \end{aligned}\right\} \tag{28}$$

Substituting these boundary conditions into equation (27) we get

$$C_1 = \frac{0.384U^{*3}}{r_o^+ \nu_g} \tag{29a}$$

and

$$C_6 = 0.259U^{*2}. \tag{29b}$$

Substituting equations (29a) and (29b) into (27), we get

$$V_g = U^*\left[0.768\left(1 - \frac{y^+}{r_o^+}\right) + 0.518\right]^{1/2} \tag{30}$$

V_g can be written as a function of time, using equations (24) and (29a) as

$$V_g = \frac{0.384U^{*3}t}{r_o^+ \nu_g} + 0.72U^*. \tag{31}$$

The mean r.m.s. velocity can be evaluated by integrating equation (30) with respect to y^+ to get

$$\bar{V}_g = 0.923U^*. \tag{32}$$

The plotting of equation (30) in Fig. 1 (shown by small dashed lines) shows a good agreement with Laufer's measurements [21].

2.5. *Solution technique*

Equation (20) was used to find the local value of $w = V_g - V_p$. Then by using equation (31), the local value of V_g was determined. Looking at equation (20), one can find the local value of V_p and then from (9) find δ. Finally, substituting into equation (8), one can determine the value of k_d/U^*.

In many practical situations, the suspended droplets may not be of uniform size, but have a size distribution. In such cases, an appropriate mean diameter has to be specified for evaluating τ^+. The arithmetic mean drop size is taken as the effective droplet diameter in the present calculations.

3. PREDICTION OF PARTICLE DIFFUSIVITY RATIO

Using equations (20), (31) and (9), we can evaluate δ at different values of Re and τ^+. The latter parameter is given in equation (22). The results are plotted in Fig. 2, which shows the following observations.

At constant Re, as τ^+ increases, δ decreases.

At constant τ^+, as Re increases, δ increases.

The usefulness of this graph is that one can easily find δ at any given condition, i.e. if we know τ^+ and Re, we can find δ.

4. COMPARISON WITH EXPERIMENTAL DATA

The accuracy of the proposed theory is now tested by comparing the calculated results with the existing experimental data as well as with the present measurements.

4.1. *Deposition data for monodisperse particles*

Much of the deposition data in the literature was obtained using monodisperse particles. Such data are not associated with uncertainties in particle size and therefore present an excellent basis for comparison with theory. For monodisperse particles, the present theory can be compared with the reliable data of Agarwal [6] over a wider range of Re and τ^+, with a few data points of Sehmel [2] and Liu and Ilori [22] within a narrow range of τ^+ between 40 and 60, and finally with the data of Ganić and Mastanaiah [1] with the drop size distribution.

Deposition data of Agarwal [6]. Agarwal [6] has obtained deposition data for uniform-size, uranine-tagged olive aerosol in a vertical down-flow of air in a 3.27-mm-I.D. glass tube with $L/D = 91.7$ at $Re = 6000$, and in a 13.8-mm-I.D. copper tube with $L/D = 73.9$ at $Re = 50\,000$. The test section tubes are smooth. The drops are generated by means of a vibrating orifice monodisperse aerosol generator. The maximum size of the droplets used is 21 μm, and the droplet to fluid density ratio is about 713. The deposition velocity is determined from the amount of aerosol deposited on the deposition section only and hence no entrance effects are present.

The calculated deposition velocity k_o/U^* vs τ^+ using the present analysis is compared with ref. [6] in Figs. 3 and 4, which show only data for $\tau^+ > 40$. The results calculated from the theories of Friedlander and Johnstone [9] and Ganić and Mastanaiah [1] are also given. It is clear that the theory of Friedlander and Johnstone

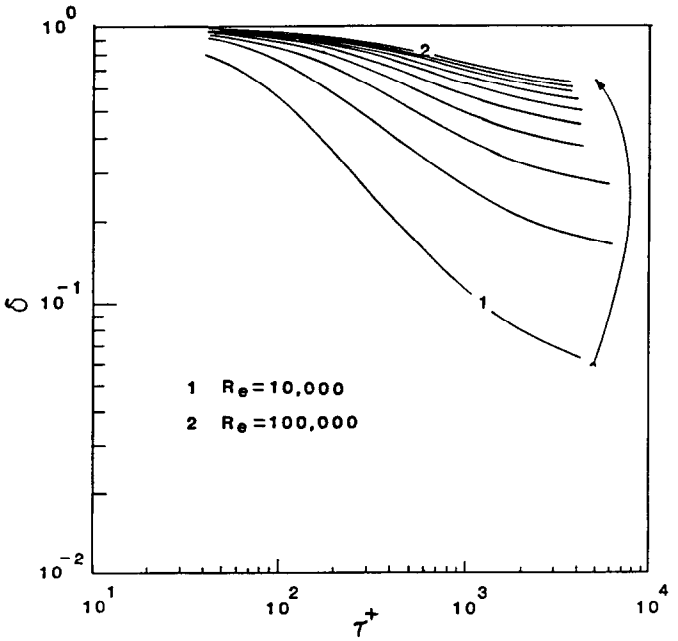

FIG. 2. Prediction of the diffusivity ratio δ as a function of τ^+, at different values of Re starting with $Re = 10\,000$ with increment 10 000, ending with $Re = 100\,000$.

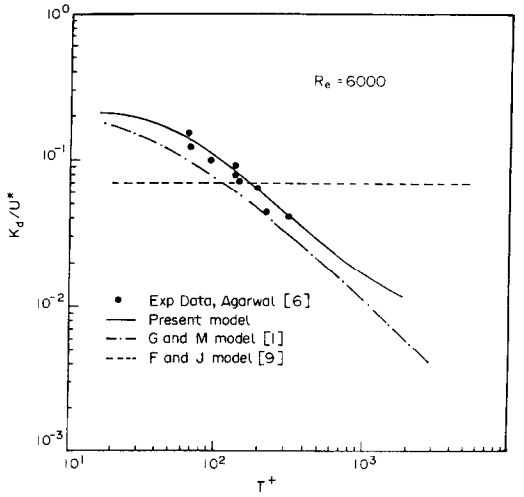

FIG. 3. Comparison of predicted deposition velocity with the experimental data of Agarwal [6].

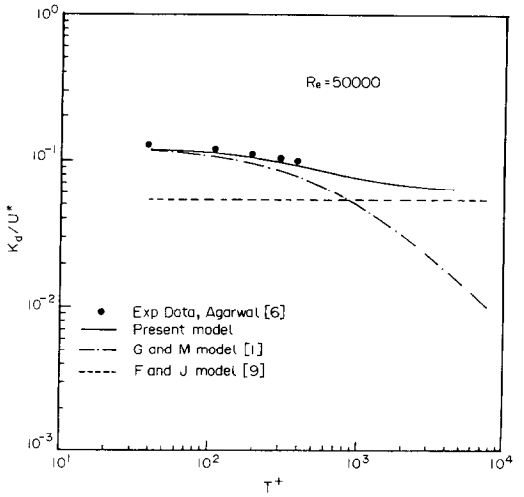

FIG. 4. Comparison of predicted deposition velocity with the experimental data of Agarwal [6].

[9] was unable to predict the deposition velocity and that of Ganić and Mastanaiah [1] slightly underpredicts the measurements. However, the present model represents the best prediction for the experimental data, as it takes into account the presence of the inertia forces of fluid (Oseen regime).

Deposition data of Sehmel [2] *and Ilori* [3]. Sehmel [2] has obtained deposition data in an upward, vertical flow of air and methylene blue aerosol in 71- and 29-mm-I.D. tubes. The maximum particle diameters used are 28 and 8.5 μm for the larger and smaller diameter tubes, respectively. The data of Ilori [3] are obtained in an upward, vertical flow of air and 80% methylene–20% uranine in a 29.8-mm vertical tube at $Re = 50\,000$. The droplet to fluid density ratio is about 1317 and the size of the droplets is of the order of 6.9 μm.

The present theory, the theory of Friedlander and Johnstone [9], and the theory of Ganić and Mastanaiah [1] are compared in Table 1 with the data of Sehmel [2] and Ilori [3]. It is evident that the present theory is in satisfactory agreement with the data, while the theory of Friedlander and Johnstone [9] considerably underpredicts the data. It can also be noticed that the present theory has better agreements than that of Ganić and Mastanaiah [1].

Deposition data of Ganić and Mastanaiah [1]. Ganić and Mastanaiah [1] have obtained deposition data in an upward, vertical flow of air and water in 12.7-mm-I.D. acrylic tubes. The maximum particle diameter used is 45 μm. The present theory, Ganić–Mastanaiah theory [1], and the theory of Friedlander and Johnstone [9] are compared in Figs. 5 and 6. The present theory shows good agreement, as does that of Ganić and Mastanaiah [1] up to $\tau^+ = 800$ ($Re = 94\,600$). The present theory, however, follows the profile of the plotted experimental data better.

4.2. *Present deposition measurements*

Experimental apparatus and procedure. In order to provide a further check on the proposed deposition model, the theory is also compared with the present deposition data. The authors have recently obtained deposition rate measurements for an air–water system in a vertical tube at near atmospheric pressure using the same apparatus used by Mastanaiah [14]; details

Table 1. Comparison of predicted deposition velocities with the experimental data of Sehmel [2] and Ilori [3]

					k_d/U^*				% Error			
Ref.	D (mm)	d_p (μm)	Re	τ^+	Exp.	Present theory	G–M*	F–J†	Present theory	G–M	F–J	Re_d
[2]	71	28.0	35000	40	0.16	0.1256	0.123	0.054	21	23.1	66.2	0.05
	29	8.5	60000	55	0.12	0.1123	0.110	0.050	6.4	8.3	58.8	0.04
[3]	29.8	9.0	50000	48	0.12	0.116	0.114	0.051	3.3	5	57.5	0.05

* G–M: theory of Ganić and Mastanaiah [1].
† F–J: theory of Friedlander and Johnstone [9].

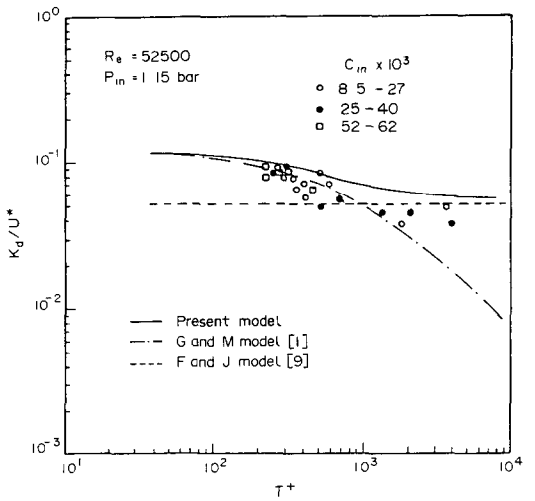

FIG. 5. Comparison of predicted deposition velocity and the experimental data of Mastaniah [14].

of the experiments are given in this reference. The Sauter mean diameter of droplet size distribution d_{32} is calculated from the Nukiyama–Tanasawa correlation [23], which gives a good agreement with the measured drop size done by Mastanaiah. The values of d_{10} are obtained from d_{32}, using the relations for the drop diameter developed by Tatterson *et al.* [24]. The technique of measuring the deposition rate is similar to that applied by Cousins and Hewitt [7]. During the experiment, the liquid layer formed at the inlet of the test section is completely removed. The drops then migrate towards the wall and form a thin liquid film that grows continuously along the test section. The liquid film formed at the test section exit is also removed completely. The flow rate of liquid collected at the test section exit gives the amount of liquid deposited over the entire test section length and thence the fractional deposition F. With a knowledge of F, the deposition velocity k_d is determined from

$$F = 1 - \exp[-4(k_d/\bar{U})(L/D)]. \quad (33)$$

The absence of entrainment for the present experimental conditions is confirmed using the correlations of Troung and Huyghe [25], which suggest entrainment E of less than 0.5% for $Re = 55\,200$. In view of these factors the entrainment effect is not taken into account in deducing the deposition velocities. The flow rate of air removed through the extractor is, however, measured to be less than about 1% of the total air flow rate through the test section and is therefore considered to have no significant effect on the measured deposition data. An error analysis done by Mastanaiah [14] has indicated that the measured deposition velocities are accurate to within about 12%. The reproducibility of the data has been assured by repeating some of the runs. The data in general are consistent without significant scatter and are therefore considered reliable.

Comparison of data obtained from the theory with that of the experimental work. The measured dimensionless deposition velocity for $Re = 26\,700$, 36 000, 43 000 and 55 200 are depicted in Figs. 7–10. The conditions for a different set of data are given in Table 2. It can be shown in Fig. 7 that k_d/U^* decreases with τ^+ beyond which it remains nearly independent of τ^+. This trend is also noticed in practically all experimental data. The physical reason for this effect is that as τ^+ increases, the droplet size increases, and the weight also increases, so the droplet becomes too heavy to follow the flow. Up to a certain size, the

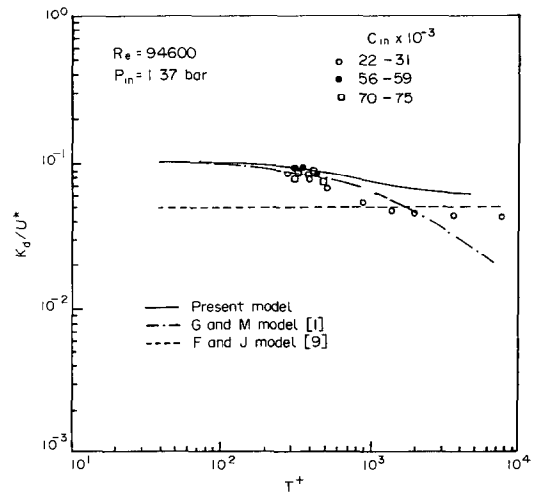

FIG. 6. Comparison of predicted deposition velocity with the experimental data of Mastaniah [14].

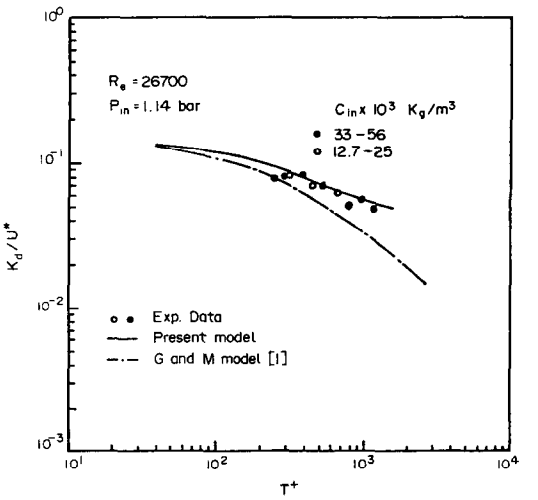

FIG. 7. Comparison of predicted deposition velocity with the present experimental data at $Re = 26\,700$; gas flow rate $w_g = 5.05 \times 10^{-3}$ kg s^{-1}; liquid loading $w_l = 2.5 \times 10^{-3}$ kg s^{-1}, 01.79×10^{-3} kg s^{-1}.

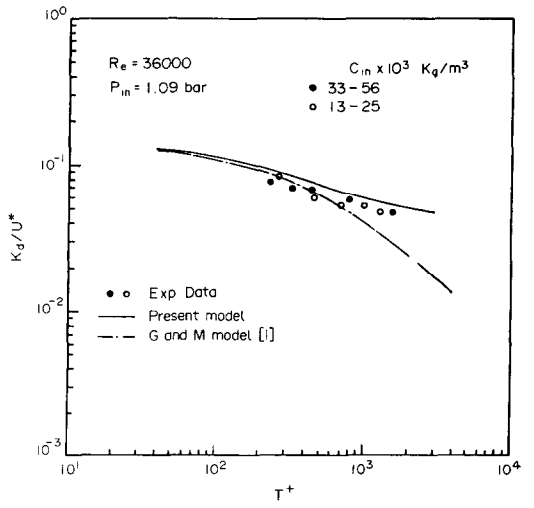

FIG. 8. Comparison of predicted deposition velocity with the present experimental data at $Re = 36000$; gas flow rate $w_g = 6.649 \times 10^{-3}$ kg s^{-1}, liquid loading $w_l = 1.135 \times 10^{-3}$ kg s^{-1}, 01.794×10^{-3} kg s^{-1}.

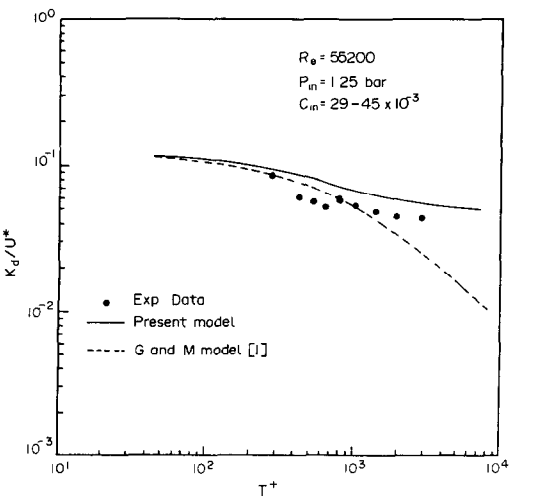

FIG. 10. Comparison of predicted deposition velocity with the present experimental data at $Re = 55200$; gas flow rate $w_g = 10.17 \times 10^{-3}$ kg s^{-1}; liquid loading $w_l = 1.79 \times 10^{-7}$ kg s^{-1}.

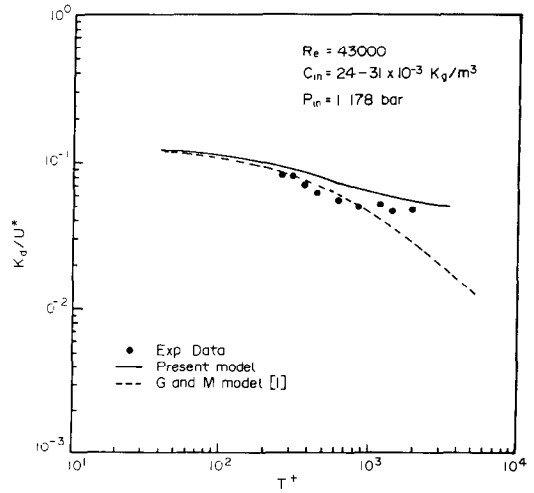

FIG. 9. Comparison of predicted deposition velocity with the present experimental data at $Re = 43000$; gas flow rate $w_g = 7.96 \times 10^{-3}$ kg s^{-1}; liquid loading $w_l = 1.79$ kg s^{-1}.

momentum of the particle will compensate for the decrease in velocity, attaining almost the same deposition rate without dependency on τ^+.

The prediction of k_d/U^* from the present theory, and the theory of Ganić and Mastanaiah [1], are also compared in Figs. 7–10. It is observed from Fig. 7 that the present theory is in good agreement with the data, an even has the same trend.

In Fig. 8, the present theory overestimated over the entire range. This is due to experimental error which was estimated at 12%, while in Figs. 9 and 10 the error becomes relatively greater. The reason for this is that as *Re* increases, the air flow rate increases, causing some evaporation from the liquid deposited on the wall, thus resulting in the smaller amount of water deposition measured.

In view of the above comparisons, it is evident that the present theory offers a considerable improvement over previous theories for $Re_p \leqslant 5$.

Table 2. The conditions for experimental data obtained

Re	Inlet pressure (bar)	d_{10} (μm)	$\bar{C}_{in} \times 10^{-3}$ (kg m^{-3})	τ^+ Oseen regime	τ^+ Stokes regime
26790	1.09	22.8–53.13	12.7–56.8	251–1180	308–1632
36040	1.134	17—50	15–36	235–1522	285–2367
43150	1.185	15.5–51	24–31	258–1965	316–3240
55230	1.254	14–53	29–45	279–2817	346–5108

5. DISCUSSION AND CONCLUSION

It can be shown that k_d/U^* is a function of Re, τ^+ and ρ_p/ρ_g since

(a) w [equation (20)] is a function of a and b, which means a function of droplet diameter and ρ_p/ρ_g, so that $w = f(\tau^+, \rho_p/\rho_g)$.
(b) Also δ is a function of V_g and w, and V_g is a function of Re, then $\delta = f(\tau^+, Re, \rho_p/\rho_g)$.
(c) From equation (8), k_d/U^* is a function of δ, Re and τ^+. Therefore, $k_d/U^* = f(Re, \tau^+, \rho_p/\rho_g)$.

The proposed expression for deposition velocity given by equation (8), using the value of δ by interpolation from Fig. 2, is believed to be of considerable application in predicting droplet deposition rates in a two-phase flow. The Oseen drag force produces a better prediction for evaluating the droplet deposition and is valid for a wide range of values for d_p and τ^+. This better predictability should be important in a wide range of applications of the two-phase flow.

Acknowledgement—This work was supported by the National Science Foundation under grant CME-8005681.

REFERENCES

1. E. N. Ganić and K. Mastanaiah, Investigation of droplet deposition from a turbulent gas stream, *Int. J. Multiphase Flow* **7**, 401–422 (1981).
2. G. A. Sehmel, Aerosol deposition from turbulent air stream in vertical conduits, Pacific Northwest Laboratory Rep. BNWL-578 (1968).
3. T. A. Ilori, Turbulent deposition of particles inside pipes. Ph.D. thesis, University of Minnesota (1971).
4. L. J. Forney and L. A. Spielman, Deposition of coarse aerosols from turbulent flow, *J. Aerosol Sci.* **5**, 257–271 (1974).
5. R. Y. H. Liu and J. K. Agarwal, Experimental observation of aerosol deposition in turbulent flow, *J. Aerosol Sci.* **5**, 145–155 (1974).
6. J. K. Agarwal, Aerosol sampling and transport. Ph.D. thesis, University of Minnesota, Particle Tech. Lab. Publ. 265 (1975).
7. L. B. Cousins and G. F. Hewitt, Liquid phase mass transfer in annular two-phase flow: droplet deposition and liquid entrainment, AERE-R5657 (1968).
8. R. A. Farmer, P. Griffith and W. M. Rohsenow, Liquid droplet deposition in two-phase flow, *Trans. Am. Soc. mech. Engrs*, Series C, *J. Heat Transfer* **92**, 587–594 (1970).
9. S. K. Friedlander and H. F. Johnstone, Deposition of suspended particles from turbulent gas streams, *Ind. Engng Chem.* **49**, 115–1156 (1957).
10. J. W. Cleaver and B. Yates, A sublayer model for the deposition of particles from a turbulent flow, *Chem. Engng Sci.* **30**, 983–992 (1975).
11. S. Namie and T. Ueda, Droplet transfer in two-phase annular mist flow: II. Prediction of droplet transfer rate, *Bull. J.S.M.E.* **16**, 752–764 (1973).
12. Y. Hagiward and T. Satao, An experimental investigation of liquid droplets diffusion in annular-mist flow, *2nd Multiphase Flow and Heat Transfer Symposium–Workshop*, Miami, FL (1979). Also published in *Multiphase Transport* (Edited by T. N. Verziroglu). Hemisphere, New York.
13. C. M. Tchen, *Mean Value and Correlation Problems Connected with the Motion of Small Particles Suspended in a Turbulent Fluid.* Martinus Nijhoff, The Hague (1947).
14. K. Mastanaiah, Experimental and theoretical investigation of droplet deposition and heat transfer in air–water dispersed flow. Ph.D. thesis, University of Illinois, Chicago Circle (1980).
15. H. Reichhardt, Vollstandige Darstellung der turbulenten Geschwindigkeitsverteilung in glatten Leitungen, *Z. angew. Math. Mech.* **31**, 208–219 (1951).
16. W. M. Kays, *Convective Heat and Mass Transfer.* McGraw-Hill, New York (1966).
17. J. O. Hinze, *Turbulence*, 2nd edn. McGraw-Hill, New York (1975).
18. P. D. McCormack and L. Grave, *Physical Dynamics.* Academic Press, New York (1973).
19. G. A. Korn and T. M. Korn, *Mathematical Handbook*, 2nd edn. McGraw-Hill, New York (1968).
20. M. M. El-Kassaby, Drop deposition and heat transfer in two-component dispersed flow. Ph.D. thesis, University of Illinois at Chicago (1982).
21. J. Laufer, The structure of turbulence in fully developed pipe flow, NACA Report 1174 (1954).
22. B. Y. H. Liu and T. A. Ilori, Aerosol deposition in turbulent pipe flow, *Envir. Sci. Technol.* **8**, 351–356 (1974).
23. S. Nukiyama and Y. Tanasawa, An experiment on the atomization of liquid by means of an air stream, Reps I and 4, *Trans. Japan Soc. mech. Engrs* **4**, 86 (1938); **5**, 68 (1939).
24. D. F. Tatterson, J. C. Dallman and T. J. Hanratty, Drop sizes in annular gas–liquid flows, *A.I.Ch.E. Jl* **23**, 68–76 (1977).
25. Q. M. Troung and J. Huyghe, Some hydrodynamical aspects of annular dispersed flow: entrainment and film thickness, Symposium on Two-Phase Flow, paper C2, Exeter, U.K. (1965).

DEPOT DE GOUTTELETTES DANS UN ECOULEMENT TURBULENT DIPHASIQUE

Résumé—Des études théoriques et expérimentales ont été conduites sur le dépôt de particules, à partir d'un écoulement turbulent diphasique, sur la paroi lisse d'un tube vertical. Les travaux de Ganic et Mastanaiah [8] pour le régime de Stokes a été étendu jusqu'à inclure le régime d'Oseen ($Re_p \leq 5$). La théorie proposée décrit correctement les données connues aussi bien que de nouvelles données relatives à un écoulement air-gouttelettes d'eau qui passe dans un tube d'acier inoxydable de 12,95 mm de diamètre, à $Re = 27\,000$, 36 000, 43 000 et 55 000.

TROPFENABLAGERUNG IN EINER TURBULENTEN ZWEIPHASENSTRÖMUNG

Zusammenfassung—Es wurden theoretische und experimentelle Untersuchungen zur turbulenten Ablagerung von Partikeln aus einer zweiphasigen Tropfenströmung an die glatte Wand eines senkrechten Rohres durchgeführt. Die Arbeit von Ganic und Mastanaiah für den Stokes-Bereich wurde durch diese Untersuchung erweitert, indem der Oseen Bereich ($Re_p \leqslant 5$) mit einbezogen wurde. Die vorgeschlagene Theorie beschreibt die vorhandenen Daten und ebenso die neuen Daten, die an einer Luft–Wasser Tropfenströmung ermittelt wurden, welche durch ein Rohr mit 12,95 mm Durchmesser aus rostfreiem Stahl bei $Re = 27\,000$, 36 000, 43 000 und 55 000 strömt.

ОСЕДАНИЕ КАПЕЛЬ В ДВУХФАЗНОМ ТУРБУЛЕНТНОМ ПОТОКЕ

Аннотация—Теоретически и экспериментально исследовано турбулентное оседание частиц из двухфазного потока на гладкую стенку вертикальной трубы. Результаты Ганича и Мастаньяха [8] для режима Стокса распространены на режим Озеена ($Re_p \leqslant 5$). Предложенная теория удовлетворительно описывает известные данные, а также результаты, полученные для капельного потока воздух–вода в нержавеющей стальной трубе с диаметром 12,95 мм при $Re = 27000$, 36000, 43000 и 55000.